Noniterative isobar diagrams and their effect in NN scattering

K. Holinde and R. Machleidt

Institut für Theoretische Kernphysik der Universität Bonn, Nussallee 14-16, D-5300 Bonn, West Germany

Amand Faessler and H. Müther

Institut für Theoretische Physik der Universität Tübingen, Auf der Morgenstelle 14, D-7400 Tübingen, West Germany

M. R. Anastasio

Brooklyn College of CUNY, Brooklyn, New York 11210

The fourth-order noniterative diagrams involving nucleon-isobar intermediate states and including π exchange are calculated in momentum space in the framework of noncovariant perturbation theory. A potential model is presented which includes, apart from these diagrams, suitable one-boson-exchange terms and iterative isobar diagrams involving $N\Delta$- and $\Delta\Delta$-intermediate states, considering π and ρ exchange for the transition potentials. Finally, noniterative two-π-exchange diagrams involving two-nucleon intermediate states are also taken into account. Such a model is able to describe NN scattering phase shifts satisfactorily. The role of the different parts of the potential model in NN scattering is studied.

> NUCLEAR STRUCTURE   Nucleon-nucleon interaction, noniterative π exchange, intermediate $N\Delta$ states, crossed-box diagrams, NN phase shifts.

I. INTRODUCTION

The simplest model of nuclear matter is a collection of point nucleons interacting through a realistic two-body potential that fits the two-nucleon data, i.e., the phase shifts for nucleon-nucleon (NN) scattering and the deuteron. In fact, starting from the phenomenological Reid-soft-core (RSC) potential[1] and in the framework of the Brueckner-Bethe theory,[2] a reasonable description of the empirical nuclear matter properties (binding energy and density) could be obtained.[3] A recent reexamination of three-body and higher-order terms[4] showed, however, that the predicted binding energy and saturation density are definitely too high. This fact is also supported by new variational calculations in the Fermi-hypernetted-chain (FHNC) approximation.[5]

On the other hand, the RSC potential underbinds light nuclei, e.g., the triton[6] and ^{16}O,[7] unless one assumes large contributions arising from three-body forces in finite nuclei, which seems to be not very realistic.[8] Therefore, the picture of nuclear matter being solely a collection of nucleons is obviously too simple; the resulting binding energy grows too strongly with the density.

Furthermore, there are meson-theoretical arguments[9] as well as empirical evidence[10] that the tensor force in the RSC potential is too strong. This is very important since the calculated binding energy of nuclear systems is very sensitive to the amount of tensor force present in the NN interaction, namely, the binding energy in-

creases with decreasing tensor force. This is clear from the property of the tensor force contributing to the binding energy mainly via second-order contributions, which are suppressed in the medium because of Pauli and dispersion effects. This argument also explains why this effect is strongly density dependent.

Thus, realistic NN potentials with reasonably small tensor force might ultimately be able to describe the binding energies of light nuclei in a satisfactory way. They will, however, grossly overbind nuclear matter. Obviously, in order to get reasonable results, consistent for all densities, additional (attractive) tensor-type contributions of relatively short range are needed, which are suppressed in the medium for higher densities only.

In a meson-theoretic framework, such contributions arise naturally from an explicit description of the 2π exchange, which mainly supplies the intermediate-range attraction. It can be split up into the diagrams shown in Fig. 1. Here N denotes an intermediate-nucleon state, whereas Δ represents an intermediate Δ isobar. The last two terms in this figure show typical rescattering contributions.

In one-boson-exchange (OBE) models,[11] the intermediate-range attraction is described phenomenologically by the exchange of a more or less fictitious scalar isoscalar σ meson. This contribution effectively replaces the $(J^P = 0^+, I = 0)$ part of the whole 2π exchange (Fig. 1) minus the twice-iterated one-pion-exchange (OPE) [which is already in-
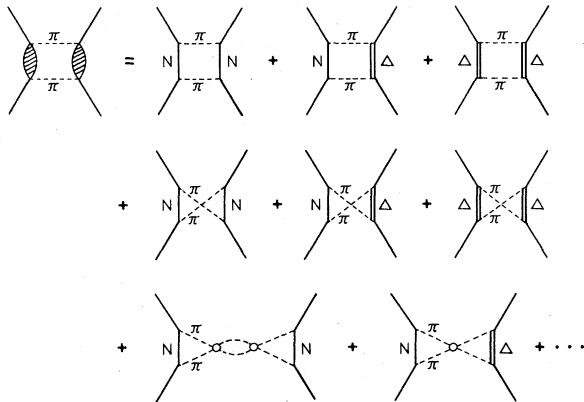
FIG. 1. 2π-exchange diagrams.

cluded in the scattering amplitude by iterating the one-pion-exchange potential (OPEP)]. On the other hand, dispersion-theoretic methods obtain this contribution by using empirical πN (and $\pi\pi$) data and performing an analytic continuation.[12]

However, both methods treat this contribution as part of the NN potential (of essentially scalar type), i.e., as a lowest-order contribution. Thus, the modifications of the diagrams in Fig. 1 in the medium, due to Pauli and dispersion effects, which arise in a nuclear many-body theory, are suppressed, apart from the nucleon box diagram which is treated as a second iteration of the OPEP. These many-body effects should be important, especially in dense systems like nuclear matter or, even more, in neutron stars.

The first study of such modifications were made for the isobar box diagrams by treating them as second iteration of so-called transition potentials $V(NN\rightarrow N\Delta)$ and $V(NN\rightarrow\Delta\Delta)$. In order to obtain such potentials one starts from a suitably defined Lagrangian-density coupling for the $N\Delta\pi$ vertex, uses the static limit, and neglects the Δ-N mass difference.[13] The resulting transition potentials are very similar to the usual OPEP, i.e., they contain strong tensor forces. Therefore, this procedure replaces part of the scalar potential (provided, e.g., by σ exchange) by second iterations of tensor force contributions, which are shorter ranged than OPE tensor force due to the higher mass of the Δ compared to the nucleon. As discussed above, this just seems to be needed in order to get consistent results for light and heavy nuclei.

Recently, however, it was pointed out by the Stony Brook group[14] that in the derivation of a suitable transition potential, the Δ-N mass difference ($\simeq 300$ MeV) together with relativistic effects cannot be neglected, since they make the isobar box diagrams shorter ranged and reduce them by a factor of 2–3. In other words, usual transition potentials grossly overestimate the contribution of the isobar box diagrams to the intermediate-range attraction of the NN interaction. Therefore, a careful relativistic treatment is needed in order to describe the isobar contribution in a realistic way. This suggests that one does the whole calculation in momentum space, which makes it possible to keep the full structure of the $N\Delta$ vertex.

Moreover, one should realize that corresponding modifications occur also in the crossed diagrams (second row in Fig. 1), which cannot be built up by a second iteration of some transition potential. The treatment of such modifications requires a much more explicit dynamical scheme, which starts from a field-theoretical Hamiltonian containing as its basic ingredient not a potential, but NN and $N\Delta$ vertices (for details see Ref. 9).

We have recently studied the isobar box diagrams within this extended scheme and in momentum space, including π and ρ exchange at the $N\Delta$ vertices, in NN scattering[15] and in nuclear matter.[16] We confirmed the results found by the authors of Ref. 14 concerning the overestimation of isobar contributions. In our case, the isobar box diagrams provide roughly 30% of the intermediate-range attraction. Without modifications, such contributions would give about 36 MeV binding at empirical nuclear matter density ($k_F \simeq 1.4$ fm^{-1}). (The total intermediate-range attraction of the NN potential yields about 100 MeV binding.) Pauli and dispersive effects, however, reduce the contribution from isobar box diagrams from 36 to 24 MeV, i.e., by as much as $\simeq 30\%$.

In a next step[17,18] we have performed corresponding calculations for the noniterative diagrams involving NN-intermediate states and including π exchange (represented by the first term in the second row of Fig. 1). It turned out that those diagrams contribute roughly 10% to the attraction in NN scattering. Therefore, neglecting modifications in the medium, they would contribute roughly 10 MeV to the binding at empirical nuclear matter density. In this case, the quenching of the diagrams in the medium is, however, relatively small (due to their short range), but cannot be neglected: many-body effects reduce them by only 20% (compared to 30% in the case of isobar box diagrams) at $k_F = 1.4$ fm^{-1}. Nevertheless, the effect grows strongly with the density.

The main aim of the present paper is to evaluate the noniterative diagrams involving one intermediate Δ. Although we expect the many-body modifications to be of the order of only 10% (they should be of even shorter range than those with NN-intermediate states), these diagrams are important in order to generate the essentially isoscalar behav-
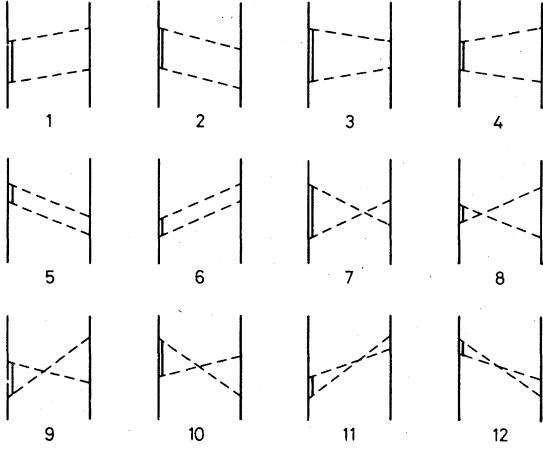
FIG. 2. Time-ordered diagrams with positive-energy
$N\Delta$ intermediate states.

ior of the total isobar contribution, as pointed out
in Ref. 14.

Section II contains the basic features of our
scheme. In Sec. III, we evaluate the diagrams in
question. The results are presented and discussed
in Sec. IV. A short summary is given in Sec. V.

II. THE SCHEME

In this section, we shortly sketch our dynamical
scheme. Details may be found in Refs. 9 and 19.
We start from a Hamiltonian

$$H = H_0 + W, \tag{2.1}$$

with

$$H_0 = h_0 + t = h_0^{(N)} + h_0^{(\Delta)} + t, \tag{2.2}$$
$$W = W^{(N)} + W^{(\Delta)},$$

where

$$h_0^{(N)} = \sum_\alpha E_\alpha^{(N)} a_\alpha^\dagger a_\alpha,$$

$$h_0^{(\Delta)} = \sum_{\alpha'} E_{\alpha'}^{(\Delta)} c_{\alpha'}^\dagger c_{\alpha'},$$

$$t = \sum_k \omega_k b_k^\dagger b_k, \tag{2.3}$$

$$W^{(N)} = \sum_{\alpha\alpha'k} W_{\alpha\alpha'k}^{(N)} a_{\alpha}^\dagger a_\alpha b_k + \text{H.c.},$$

$$W^{(\Delta)} = \sum_{\alpha\alpha'k} W_{\alpha\alpha'k}^{(N)} c_{\alpha'}^\dagger a_\alpha b_k + W_{\alpha\alpha'k}^{(\Delta)} c_{\alpha'}^\dagger a_\alpha b_k^\dagger + \text{H.c.}.$$

Here, $a_\alpha^\dagger$, $c_{\alpha'}^\dagger$, and $b_k^\dagger$ are the creation operators
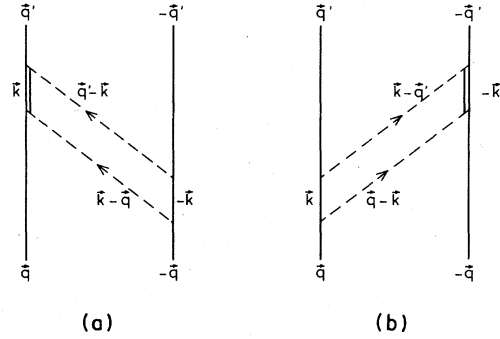

(a)   (b)

FIG. 3. Selected stretched-box diagrams displaying
the notation as it is used in the text.

for nucleons, isobars, and bosons, respectively;
$E_\alpha^{(N)}$, $E_{\alpha'}^{(\Delta)}$, and ω_k are the corresponding relativ-
istic kinetic energies. α, α', and k denote all
quantum numbers which specify the state complete-
ly. $W_{\alpha\alpha'k}^{(N)}$ represents the nucleon-nucleon-meson
vertices, whereas $W_{\alpha\alpha'k}^{(\Delta)}$ and $W_{\alpha\alpha'k}^{(\Delta)'}$ describe the
nucleon-isobar-meson vertices.

Note that we neglect antiparticles from the be-
ginning. This is justified since the $N\overline{N}$ vertex is
considerably suppressed compared to the NN ver-
tex because of chiral invariance and pair suppres-
sion[20] and also due to quark model arguments.[21]

We treat W in old-fashioned, noncovariant pertur-
bation theory. This seems to be an adequate pro-
cedure because old-fashioned perturbation theory
corresponds to standard nonrelativistic many-body
theory and will, therefore, allow a direct com-
parison with the usual procedure in a many-body
theory. Then the nucleon-nucleon scattering am-
plitude T can be represented by a series expansion
defined by all diagrams containing two ingoing and
two outgoing nucleon lines. Since we use physical
masses, we have to leave out self-energy dia-
grams in order to avoid double counting. This se-
ries can be partially summed by solving an inte-
gral equation of Lippmann-Schwinger type,

$$T(z) = V_{\text{eff}}(z) + V_{\text{eff}}(z)\frac{1}{z - h_0^{(N)}} T(z). \tag{2.4}$$

Here, z is the (relativistic) starting energy for
free two-body scattering. The energy-dependent
quasipotential $V_{\text{eff}}(z)$ contains the (infinite) sum of
all diagrams with at least one meson or one Δ iso-
bar present in each intermediate state.

Considering only diagrams up to fourth order in
W, $V_{\text{eff}}(z)$ can be represented as

$$V_{\text{eff}}(z) = W^{(N)}\frac{1}{z - h_0^{(N)} - t} W^{(N)} + W\frac{1}{z - h_0 - t} W\frac{1}{z - h_0 - t} W\frac{1}{z - h_0 - t} W$$
$$- W^{(N)}\frac{1}{z - h_0^{(N)} - t} W^{(N)}\frac{1}{z - h_0^{(N)}} W^{(N)}\frac{1}{z - h_0^{(N)} - t} W^{(N)}. \tag{2.5}$$

The first term gives the OBE part. The second term describes the fourth-order diagrams involving NN, ΔN, $N\Delta$, and $\Delta\Delta$ intermediate states, shown in Fig. 2 for ΔN intermediate states only. The last term in Eq. (2.5) eliminates the iterative diagrams with NN intermediate states, which are already included by iterating the OBE part in Eq. (2.4).

III. NONITERATIVE ISOBAR DIAGRAMS

The first four (iterative) isobar diagrams of Fig. 2 were already evaluated in Ref. 15. Here, we present the analogous calculations for the noniterative, i.e., stretched-box (5 and 6) and crossed-box (7–12) diagrams. The diagrams with NN intermediate states are treated in Ref. 17.

We start with the usual interaction Lagrangian

$$L_{NN\pi} = \sqrt{4\pi}\,g_\pi i\bar{\psi}\vec{\tau}\gamma^5\psi\vec{\phi}\,,$$

$$L_{N\Delta\pi} = \sqrt{4\pi}\,\frac{f_{N\Delta\pi}}{m_\pi}\,\bar{\psi}\vec{T}\psi^\mu\partial_\mu\vec{\phi} + \text{H. C.}\,, \tag{3.1}$$

where g_π is the pion-nucleon coupling constant, $f_{N\Delta\pi}$ is the coupling constant at the $N\Delta$ vertex, and m_π is the pion mass. Here ψ denotes the nucleon field operator, ϕ denotes the pion field, ψ^μ denotes the field operator of the Δ isobar, and $\vec{\tau},\vec{T}$ are the isospin matrices.

The Lagrangians (3.1) suggest the following form for the corresponding vertex functions:

$$W^{(N,\pi)}_{\alpha'\alpha k} = -\frac{\sqrt{4\pi}g_\pi}{[2\omega_k\,(2\pi)^3]^{1/2}}\,\delta(\vec{q}_{\alpha'} - \vec{q}_\alpha - \vec{k})\bar{u}_{r_{\alpha'}}(\vec{q}_{\alpha'})i\gamma^5 u_{r_\alpha}(\vec{q}_\alpha) \tag{3.2}$$

and

$$W^{(\Delta,\pi)}_{\alpha'\alpha k} = -\sqrt{4\pi}\,\frac{f_{N\Delta\pi}}{m_\pi}\,\frac{1}{[2\omega_k(2\pi)^3]^{1/2}}\,\delta(\vec{q}_{\alpha'} - \vec{q}_\alpha - \vec{k})ik_\mu\bar{u}^\mu_{r_{\alpha'}}(\vec{q}_{\alpha'})u_{r_\alpha}(\vec{q}_\alpha)\,, \tag{3.3}$$

where $\omega_k = (\vec{k}^2 + m_\pi^2)^{1/2}$ and $k_\mu \equiv (0, -\vec{k})$. The Dirac spinors u_r are normalized to $u_r^\dagger u_r = 1$ and u^μ is the Rarita-Schwinger spinor describing the isobar. $W^{(\Delta,\pi)'}_{\alpha'\alpha k}$ is obtained from $W^{(\Delta,\pi)}_{\alpha'\alpha k}$ by changing the overall sign and, in addition, $\vec{k}$ to $-\vec{k}$ in the δ function.

A. Stretched-box diagrams

One of the two noniterative box (stretched-box) diagrams is shown for convenience in Fig. 3(a), including notation. Using Eqs. (3.2) and (3.3) together with (2.5), it is written in a helicity-state basis,

$$\langle\vec{q}'\Lambda_1'\Lambda_2'|M_1^b(z)|\vec{q}\Lambda_1\Lambda_2\rangle = \frac{(4\pi)^2}{(2\pi)^6}\,g_\pi^{\,2}\frac{f_{N\Delta\pi}^{\,2}}{m_\pi^{\,2}}\,(2 + \tfrac{2}{3}\vec{\tau}_1\cdot\vec{\tau}_2)$$

$$\times\sum_{h_1^*,h_2}\int\frac{d^3k\,\bar{u}_{\Lambda_2'}(-\vec{q}')i\gamma^5 u_{h_2}(-\vec{k})\,\bar{u}_{h_2}(-\vec{k})\,i\gamma^5 u_{\Lambda_2}(-\vec{q})F_{NN\pi}[(\vec{q}'-\vec{k})^2]F_{NN\pi}[(\vec{q}-\vec{k})^2]}{4\omega_{q-k}\omega_{q'-k}}$$

$$\times\frac{\bar{u}_{\Lambda_1'}(\vec{q}')i(q'-k)_\mu u^\mu_{h_1^*}(\vec{k})\bar{u}^\nu_{h_1^*}(\vec{k})i(k-q)_\nu u_{\Lambda_1}(\vec{q})F_{N\Delta\pi}[(\vec{q}'-\vec{k})^2]F_{N\Delta\pi}[(\vec{q}-\vec{k})^2]}{(z - E_{q'} - E_k^* - \omega_{q'-k})(z - E_{q'} - E_q - \omega_{q'-k} - \omega_{q-k})(z - E_k - E_q - \omega_{q-k})}\,, \tag{3.4}$$

where $E_q = (\vec{q}^2 + m^2)^{1/2}$, $E_q^* = (\vec{q}^2 + m_\Delta^2)^{1/2}$, m is the mass of the nucleon ($= 938.9$ MeV), m_Δ is the mass of the Δ isobar ($= 1236$ MeV), and z is the starting energy. The summation goes over the helicities of the particles in the intermediate states, i.e., $h_1^* = \pm\frac{1}{2}, \frac{3}{2}$, and $h_2 = \pm\frac{1}{2}$, since the Δ isobar has spin $\frac{3}{2}$. The form factors $F_{NN\pi}$ and $F_{N\Delta\pi}$ are parametrized as

$$F_\pi[(\vec{q}' - \vec{q})^2] = \frac{\Lambda_\pi^{\,2} - m_\pi^{\,2}}{\Lambda_\pi^{\,2} + (\vec{q}' - \vec{q})^2}\,, \tag{3.5}$$

where Λ_π is a parameter, the so-called cutoff mass. The spinors are normalized such that $u^\dagger u = 1$.

The spin sum can be evaluated with the help of positive-energy nuclear projection operators

$$\Lambda_+^{(N)}(\vec{k}) = \frac{\gamma_0 E_k - \vec{\gamma}\cdot\vec{k} + m}{2E_k} \tag{3.6}$$

for the nucleon and

$$P_+^{\mu\nu}(\vec{k}) = \Lambda_+^{(\Delta)}(\vec{k})\left[-g^{\mu\nu} + \tfrac{1}{3}\gamma^\mu\gamma^\nu + \frac{2}{3}\frac{k^\mu k^\nu}{m_\Delta^2} + \frac{1}{3}\frac{\gamma^\mu k^\nu - \gamma^\nu k^\mu}{m_\Delta}\right] \tag{3.7}$$

for the Δ isobar. This gives

$$\sum_{h_2} \bar{u}_{\Lambda_2}(-\vec{q}')i\gamma^5 u_{h_2}(-\vec{k})\bar{u}_{h_2}(-\vec{k})i\gamma^5 u_{\Lambda_2}(-\vec{q}) = -\bar{u}_{\Lambda_2}(-\vec{q}')\gamma^5\Lambda_+^{(N)}(-\vec{k})\gamma^5 u_{\Lambda_2}(-\vec{q})$$

$$= \frac{1}{2E_k}\bar{u}_{\Lambda_2}(-\vec{q}')(\gamma^0 E_k + \vec{\gamma}\cdot\vec{k} - m)u_{\Lambda_2}(-\vec{q}) \tag{3.8}$$

and

$$\sum_{h_1^*}\bar{u}_{\Lambda_1}(\vec{q}')i(q'-k)_\mu u_{h_1^*}^\mu(\vec{k})\bar{u}_{h_1^*}^\nu(\vec{k})i(k-q)_\nu u_{\Lambda_1}(\vec{q})$$

$$= -(q'-k)_\mu(k-q)_\nu \bar{u}_{\Lambda_1}(\vec{q}')P_+^{\mu\nu}(\vec{k})u_{\Lambda_1}(\vec{q})$$

$$= \frac{1}{2E_k^*}\bar{u}_{\Lambda_1}(\vec{q}')(\gamma^0 E_k^* - \vec{\gamma}\cdot\vec{k} + m_\Delta)$$

$$\times\left[(\vec{q}'-\vec{k})\cdot(\vec{q}-\vec{k}) + \tfrac{1}{3}\vec{\gamma}\cdot(\vec{q}'-\vec{k})\vec{\gamma}\cdot(\vec{q}-\vec{k})\right.$$

$$\left. + \frac{2}{3}\frac{\vec{k}\cdot(\vec{q}'-\vec{k})\vec{k}\cdot(\vec{q}-\vec{k})}{m_\Delta^2} + \frac{1}{3}\frac{\vec{k}\cdot(\vec{q}-\vec{k})\gamma\cdot(\vec{q}'-\vec{k}) - \vec{k}\cdot(\vec{q}'-\vec{k})\gamma\cdot(\vec{q}-\vec{k})}{m_\Delta}\right]u_{\Lambda_1}(\vec{q}). \tag{3.9}$$

Consequently,

$$\sum_{h_1^*,h_2}\bar{u}_{\Lambda_2}(-\vec{q}')i\gamma^5 u_{h_2}(-\vec{k})\bar{u}_{h_2}(-\vec{k})i\gamma^5 u_{\Lambda_2}(-\vec{q})\bar{u}_{\Lambda_1}(\vec{q}')i(q'-k)_\mu u_{h_1^*}^\mu(\vec{k})\bar{u}_{h_1^*}^\nu(\vec{k})i(k-q)_\nu u_{\Lambda_1}(\vec{q}) = Z_1 + Z_2 + Z_3 + Z_4, \tag{3.10}$$

where

$$Z_1 = \frac{1}{4E_k E_k^*}(\vec{q}'-\vec{k})\cdot(\vec{q}-\vec{k})\bar{u}_{\Lambda_2}(-\vec{q}')(\gamma^0 E_k + \gamma\cdot\vec{k} - m)u_{\Lambda_2}(-\vec{q})\bar{u}_{\Lambda_1}(\vec{q}')(\gamma^0 E_k^* - \vec{\gamma}\cdot\vec{k} + m_\Delta)u_{\Lambda_1}(\vec{q}),$$

$$Z_2 = \frac{1}{3}\frac{1}{4E_k E_k^*}\bar{u}_{\Lambda_2}(-\vec{q}')(\gamma^0 E_k + \vec{\gamma}\cdot\vec{k} - m)u_{\Lambda_2}(-\vec{q})\bar{u}_{\Lambda_1}(\vec{q}')(\gamma^0 E_k^* - \vec{\gamma}\cdot\vec{k} + m_\Delta)\vec{\gamma}\cdot(\vec{q}'-\vec{k})\vec{\gamma}\cdot(\vec{q}-\vec{k})u_{\Lambda_1}(\vec{q}), \tag{3.11}$$

$$Z_3 = \frac{2}{3}\frac{1}{4E_k E_k^*}\frac{\vec{k}\cdot(\vec{q}'-\vec{k})\vec{k}\cdot(\vec{q}-\vec{k})}{m_\Delta^2}\bar{u}_{\Lambda_2}(-\vec{q}')(\gamma^0 E_k + \vec{\gamma}\cdot\vec{k} - m)u_{\Lambda_2}(-\vec{q})\bar{u}_{\Lambda_1}(\vec{q}')(\gamma^0 E_k^* - \vec{\gamma}\cdot\vec{k} + m_\Delta)u_{\Lambda_1}(\vec{q}),$$

$$Z_4 = \frac{1}{3m_\Delta}\frac{1}{4E_k E_k^*}\bar{u}_{\Lambda_2}(-\vec{q}')(\gamma^0 E_k + \vec{\gamma}\cdot\vec{k} - m)u_{\Lambda_2}(-\vec{q})$$

$$\times \bar{u}_{\Lambda_1}(\vec{q}')(\gamma^0 E_k^* - \gamma\cdot\vec{k} + m_\Delta)[\vec{k}\cdot(\vec{q}-\vec{k})\vec{\gamma}\cdot(\vec{q}'-\vec{k}) - \vec{k}\cdot(\vec{q}'-\vec{k})\gamma\cdot(\vec{q}-\vec{k})]u_{\Lambda_1}(\vec{q}).$$

In the following, we will describe the evaluation of Z_1 in some detail. Since we want to do the integration over $\vec{k}$ using polar coordinates, we must get rid of the $\vec{\gamma}\cdot\vec{k}$ term. Therefore, we expand $\vec{k}$ in terms of $\vec{q}$, $\vec{q}'$, and $\vec{q}'\times\vec{q}$,

$$\vec{k} = a\vec{q} + b\vec{q}' + c\frac{\vec{q}'\times\vec{q}}{|\vec{q}'\times\vec{q}|}, \tag{3.12}$$

with

$$a = \frac{\vec{q}'\cdot\vec{q}\,\vec{q}'\cdot\vec{k} - q'^2\vec{q}\cdot\vec{k}}{(\vec{q}\cdot\vec{q})^2 - q^2 q'^2}, \quad b = \frac{\vec{q}'\cdot\vec{q}\,\vec{q}\cdot\vec{k} - q^2\vec{q}'\cdot\vec{k}}{(\vec{q}\cdot\vec{q})^2 - q^2 q'^2}, \quad c = \frac{\vec{q}'\times\vec{q}}{|\vec{q}'\times\vec{q}|}\cdot\vec{k}. \tag{3.13}$$

Thus, $\gamma\cdot\vec{k}$ can be replaced by

$$\gamma\cdot k = a\gamma\cdot\vec{q} + b\gamma\cdot\vec{q}' + c\gamma\cdot\frac{\vec{q}'\times\vec{q}}{|\vec{q}'\times\vec{q}|}. \tag{3.14}$$

Using the Dirac equation, Z_1 becomes

$$Z_1 = \frac{1}{4E_k E_k^*}(\vec{q}\,' - \vec{k})\cdot(\vec{q} - \vec{k})\bar{u}_{\Lambda_2'}(-\vec{q}\,')\left[\gamma^0(E_k - aE_q - bE_{q'}) - m(1 - a - b) + c\vec{\gamma}\cdot\frac{\vec{q}\,'\times\vec{q}}{|\vec{q}\,'\times\vec{q}|}\right]u_{\Lambda_2}(-\vec{q})$$

$$\times\bar{u}_{\Lambda_1'}(\vec{q}\,')\left[\gamma^0(E_k^* - aE_q - bE_{q'}) + m_\Delta + m(a+b) - c\gamma\cdot\frac{\vec{q}\,'\times\vec{q}}{|\vec{q}\,'\times\vec{q}|}\right]u_{\Lambda_1}(\vec{q})\,. \tag{3.15}$$

If we choose $\vec{q}$ to be in the z axis and $\vec{q}\,'$ to be in the xz plane,

$$\gamma\cdot\frac{\vec{q}\,'\times\vec{q}}{|\vec{q}\,'\times\vec{q}|} = -\gamma^2\,,$$

and terms linear in c disappear after angle integration. Therefore,

$$Z_1 = \frac{1}{4E_k E_k^*}(\vec{q}\,' - \vec{k})\cdot(\vec{q} - \vec{k})\{-m(1 - a - b)[m_\Delta + m(a+b)][\bar{u}_{\Lambda_2'}(-\vec{q}\,')u_{\Lambda_2}(-\vec{q})u_{\Lambda_1'}(\vec{q}\,')u_{\Lambda_1}(\vec{q})]$$

$$+ [m_\Delta + m(a+b)](E_k - aE_q - bE_{q'})[\bar{u}_{\Lambda_2'}(-\vec{q}\,')\gamma^0 u_{\Lambda_2}(-\vec{q})\,\bar{u}_{\Lambda_1'}(\vec{q}\,')u_{\Lambda_1}(\vec{q})]$$

$$- m(1 - a - b)(E_k^* - aE_q - bE_{q'})[\bar{u}_{\Lambda_2'}(-\vec{q}\,')u_{\Lambda_2}(-\vec{q})\bar{u}_{\Lambda_1'}(\vec{q}\,')\gamma^0 u_{\Lambda_1}(\vec{q})]$$

$$+ (E_k - aE_q - bE_{q'})(E_k^* - aE_q - bE_{q'})[\bar{u}_{\Lambda_2'}(-\vec{q}\,')\gamma^0 u_{\Lambda_2}(-\vec{q})\bar{u}_{\Lambda_1'}(\vec{q}\,')\gamma^0 u_{\Lambda_1}(\vec{q})]$$

$$- c^2[\bar{u}_{\Lambda_2'}(-\vec{q}\,')\gamma^2 u_{\Lambda_2}(-\vec{q})\bar{u}_{\Lambda_1'}(\vec{q}\,')\gamma^2 u_{\Lambda_1}(\vec{q})]\}\,. \tag{3.16}$$

In order to symmetrize this expression, we do the corresponding calculations for the diagram shown in Fig. 3(b), which should give the same result. We get

$$Z_1 = \frac{1}{4E_k E_k^*}(\vec{q}\,' - \vec{k})\cdot(\vec{q} - \vec{k})\{-m(1 - a - b)[m_\Delta + m(a+b)][\bar{u}_{\Lambda_2'}(-\vec{q}\,')u_{\Lambda_2}(-\vec{q})\bar{u}_{\Lambda_1'}(\vec{q}\,')u_{\Lambda_1}(\vec{q})]$$

$$- m(1 - a - b)(E_k^* - aE_q - bE_{q'})[\bar{u}_{\Lambda_2'}(-\vec{q}\,')\gamma^0 u_{\Lambda_2}(-\vec{q})\bar{u}_{\Lambda_1'}(\vec{q}\,')u_{\Lambda_1}(\vec{q})]$$

$$+ [m_\Delta + m(a+b)](E_k - aE_q - bE_{q'})[\bar{u}_{\Lambda_2'}(-\vec{q}\,')u_{\Lambda_2}(-\vec{q})\bar{u}_{\Lambda_1'}(\vec{q}\,')\gamma^0 u_{\Lambda_1}(\vec{q}\,')]$$

$$+ (E_k - aE_q - bE_{q'})(E_k^* - aE_q - bE_{q'})[\bar{u}_{\Lambda_2'}(-\vec{q}\,')\gamma^0 u_{\Lambda_2}(-\vec{q})\bar{u}_{\Lambda_1'}(\vec{q}\,')\gamma^0 u_{\Lambda_1}(\vec{q})]$$

$$- c^2[\bar{u}_{\Lambda_2'}(-\vec{q}\,')\gamma^2 u_{\Lambda_2}(-\vec{q})\bar{u}_{\Lambda_1'}(\vec{q}\,')\gamma^2 u_{\Lambda_1}(\vec{q})]\}\,. \tag{3.17}$$

Symmetrization of Eqs. (3.16) and (3.17) then finally gives

$$Z_1 = \frac{1}{4E_k E_k^*}(\vec{q}\,' - \vec{k})\cdot(\vec{q} - \vec{k})[d_1 x_1 A_1 + (d_1 x_2 + d_2 x_1)A_2 + d_2 x_2 A_3 - c^2 A_4']\,, \tag{3.18}$$

where

$$d_1 = m(1 - a - b)\,,\quad d_2 = -(E_k - aE_q - bE_{q'})\,, \tag{3.19}$$

and

$$x_1 = -[m_\Delta + m(a+b)]\,,\quad x_2 = -(E_k^* - aE_q - bE_{q'})\,. \tag{3.20}$$

Furthermore,

$$A_1 = \bar{u}_{\Lambda_2'}(-\vec{q}\,')u_{\Lambda_2}(-\vec{q})\bar{u}_{\Lambda_1'}(\vec{q}\,')u_{\Lambda_1}(\vec{q})\,,$$

$$A_2 = \tfrac{1}{2}[\bar{u}_{\Lambda_2'}(-\vec{q}\,')\gamma^0 u_{\Lambda_2}(-\vec{q})\bar{u}_{\Lambda_1'}(\vec{q}\,')u_{\Lambda_1}(\vec{q}) + \bar{u}_{\Lambda_2'}(-\vec{q}\,')u_{\Lambda_2}(-\vec{q})\bar{u}_{\Lambda_1'}(\vec{q}\,')\gamma^0 u_{\Lambda_1}(\vec{q})]\,,$$

$$A_3 = \bar{u}_{\Lambda_2'}(-\vec{q}\,')\gamma^0 u_{\Lambda_2}(-\vec{q})\bar{u}_{\Lambda_1'}(\vec{q}\,')\gamma^0 u_{\Lambda_1}(\vec{q})\,, \tag{3.21}$$

$$A_4' = \bar{u}_{\Lambda_2'}(-\vec{q}\,')\gamma^2 u_{\Lambda_2}(-\vec{q})\bar{u}_{\Lambda_1'}(\vec{q}\,')\gamma^2 u_{\Lambda_1}(\vec{q})\,.$$

Correspondingly, one obtains for Z_2

$$Z_2 = \frac{1}{4E_k E_k^*}\tfrac{1}{3}[d_1 y_1 A_1 + (d_1 y_2 + d_2 y_1)A_2 + d_2 y_2 A_3 + c^2 y_3 A_4' + 2c^2 y_4 A_5']\,, \tag{3.22}$$

where

$$y_1 = -\{m_\Delta(aq^2 + bq'^2 - k^2) + (1 - a - b)[(E_{q'}E_q + m^2)m_\Delta + m(E_{q'} + E_q)E_k^*]$$
$$+ m[aq^2 - bq'^2 - 2a\vec{q}' \cdot (\vec{q} - \vec{k}) + 2b\vec{q}' \cdot \vec{k} - (a + b)k^2]\},$$

$$y_2 = -\{E_k^*(aq^2 + bq'^2 - k^2) - (1 - a - b)[(E_{q'}E_q + m^2)E_k^* + mm_\Delta(E_{q'} + E_q)]$$
$$+ E_q[2a\vec{q}' \cdot (\vec{q} - \vec{k}) + bq'^2 - (1 - a)k^2] - E_{q'}[aq^2 + 2b\vec{k} \cdot (\vec{q}' - \vec{k}) - (1 - b)k^2]\},$$

$$y_3 = E_k^*(E_{q'} + E_q) + 2mm_\Delta - E_{q'}E_q + m^2 - 2\vec{q}' \cdot \vec{k} + k^2,$$

$$y_4 = (m_\Delta + m)(E_{q'} - E_q),$$

(3.23)

and

$$A_5' = \tfrac{1}{2}[\bar{u}_{\Lambda_2'}(-\vec{q}')\gamma^2 u_{\Lambda_2}(-\vec{q})\bar{u}_{\Lambda_1'}(\vec{q}')\gamma^2\gamma^0 u_{\Lambda_1}(\vec{q}) + \bar{u}_{\Lambda_2'}(-\vec{q}')\gamma^2\gamma^0 u_{\Lambda_2}(-\vec{q})\bar{u}_{\Lambda_1'}(\vec{q}')\gamma^2 u_{\Lambda_1}(\vec{q})].$$

(3.24)

Obviously,

$$Z_3 = \frac{2}{3}\frac{\vec{k} \cdot (\vec{q}' - \vec{k})k \cdot (\vec{q} - \vec{k})}{m_\Delta^2}\frac{1}{4E_k E_k^*}[d_1 x_1 A_1 + (d_1 x_2 + d_2 x_1)A_2 + d_2 x_2 A_3 - c^2 A_4'],$$

(3.25)

and, finally,

$$Z_4 = \frac{1}{3m_\Delta}\frac{1}{4E_k E_k^*}[d_1 z_1 A_1 + (d_1 z_2 + d_2 z_1)A_2 + d_2 z_2 A_3 + c^2 z_3 A_4' + 2c^2 z_4 A_5'],$$

(3.26)

where

$$z_1 = \{[\vec{k} \cdot (\vec{q} - \vec{k}) + b\vec{k} \cdot (\vec{q}' - \vec{q})](E_k^* E_{q'} + mm_\Delta) - 2a\vec{q}' \cdot \vec{q}\vec{k} \cdot (\vec{q} - \vec{k})$$
$$+ [\vec{k} \cdot (\vec{q}' - \vec{k}) - a\vec{k} \cdot (\vec{q}' - \vec{q})](E_k^* E_q - mm_\Delta) - k^2\vec{k} \cdot (\vec{q}' - \vec{q})$$
$$- [a\vec{k} \cdot (\vec{q} - \vec{k}) + b\vec{k} \cdot (\vec{q}' - \vec{k})](E_{q'}E_q + m^2) + aq^2\vec{k} \cdot (\vec{q}' - \vec{k}) - bq'^2\vec{k} \cdot (\vec{q} - \vec{k})\},$$

$$z_2 = \{-[\vec{k} \cdot (\vec{q} - \vec{k}) + b\vec{k} \cdot (\vec{q}' - \vec{q})](E_k^* m + E_q m_\Delta) + [\vec{k} \cdot (\vec{q}' - \vec{k}) - a\vec{k} \cdot (\vec{q}' - \vec{q})](E_q m_\Delta - E_k^* m)$$
$$+ m(E_{q'} + E_q)[a\vec{k} \cdot (\vec{q} - \vec{k}) + b\vec{k} \cdot (\vec{q}' - \vec{k})]\},$$

$$z_3 = \{m_\Delta\vec{k} \cdot (\vec{q}' - \vec{q}) - m\vec{k} \cdot (\vec{q} - \vec{k}) - m\vec{k} \cdot (\vec{q}' - \vec{k})\},$$

$$z_4 = \{E_q\vec{k} \cdot (\vec{q}' - \vec{k}) - E_{q'}\vec{k} \cdot (\vec{q} - \vec{k}) - E_k^*\vec{k} \cdot (\vec{q}' - \vec{q})\}.$$

(3.27)

The difficult $\gamma^2\gamma^2$ term A_4' can be replaced by using

$$\gamma^2\gamma^2 = \gamma \cdot \gamma - (\gamma^1\gamma^1 + \gamma^3\gamma^3)$$
$$= \vec{\gamma} \cdot \vec{\gamma} - a'\vec{\gamma} \cdot \vec{q}'\vec{\gamma} \cdot \vec{q}' - b'(\vec{\gamma} \cdot \vec{q}'\vec{\gamma} \cdot \vec{q} + \vec{\gamma} \cdot \vec{q}\vec{\gamma} \cdot \vec{q}') - c'\vec{\gamma} \cdot \vec{q}\vec{\gamma} \cdot \vec{q},$$

(3.28)

with

$$a' = \frac{1}{q'^2\sin^2\theta}, \quad b' = -\frac{\cos\theta}{q'q\sin^2\theta}, \quad c' = \frac{1}{q^2\sin^2\theta},$$

(3.29)

where θ is the angle between $\vec{q}$ and $\vec{q}'$. Thus we obtain, using (3.28) and the Dirac equation,

$$A_4' = m^2(a' + 2b' + c')A_1 - 2m[E_{q'}a' + (E_{q'} + E_q)b' + E_q c']A_2 + (E_{q'}^2 a' + 2E_{q'}E_q b' + E_q^2 c')A_3 + A_4,$$

(3.30)

where

$$A_4 = \bar{u}_{\Lambda_2'}(-\vec{q}')\vec{\gamma}u_{\Lambda_2}(-\vec{q})\bar{u}_{\Lambda_1'}(\vec{q}')\vec{\gamma}u_{\Lambda_1}(\vec{q}).$$

(3.31)

Similarly

$$A_5' = -m[a'E_{q'} + b'(E_{q'} - E_q) - c'E_q]A_1 + [m^2(a' - c') + (a'E_{q'}^2 - c'E_q^2)]A_2$$
$$+ m[-a'E_{q'} + b'(E_{q'} - E_q) + c'E_q]A_3 + A_5,$$

(3.32)

where

$$A_5 = \tfrac{1}{2}[\bar{u}_{\Lambda_2'}(-\vec{q})\vec{\gamma}u_{\Lambda_2}(-\vec{q})\bar{u}_{\Lambda_1'}(\vec{q}')\vec{\gamma}\gamma^0 u_{\Lambda_1}(\vec{q}) + \bar{u}_{\Lambda_2'}(-\vec{q}')\vec{\gamma}\gamma^0 u_{\Lambda_2}(-\vec{q})\bar{u}_{\Lambda_1'}(\vec{q}')\vec{\gamma}u_{\Lambda_1}(\vec{q})].$$

(3.33)

The second noniterative box diagram in Fig. 2 gives essentially the same result as well as the corresponding diagrams with the isobar on the right hand side. Denoting the total contribution of these four diagrams

by M^b, we finally get

$$\langle \vec{q}'\Lambda_1'\Lambda_2'|M^b(z)|\vec{q}\Lambda_1\Lambda_2\rangle = 2\frac{(4\pi)^2}{(2\pi)^6}g_\pi^2\frac{f_{N\Delta\pi}^2}{m_\pi^2}(2+\tfrac{2}{3}\vec{\tau}_1\cdot\vec{\tau}_2)$$

$$\times\int\frac{d^3k(Z_1+Z_2+Z_3+Z_4)F_{NN\pi}[(\vec{q}'-\vec{k})^2]F_{NN\pi}[(\vec{q}-\vec{k})^2]F_{N\Delta\pi}[(\vec{q}'-\vec{k})^2]F_{N\Delta\pi}[(\vec{q}-k)^2]}{4\omega_{q-k}\omega_{q'-k}D^b}\,,$$

(3.34)

with

$$\frac{1}{D^b}=\frac{1}{D_1^b}+\frac{1}{D_2^b}\,,$$

$$D_1^b=(z-E_{q'}-E_k^*-\omega_{q'-k})(z-E_{q'}-E_q-\omega_{q'-k}-\omega_{q-k})(z-E_k-E_q-\omega_{q-k})\,,$$

$$D_2^b=(z-E_{q'}-E_k-\omega_{q'-k})(z-E_{q'}-E_q-\omega_{q'-k}-\omega_{q-k})(z-E_k^*-E_q-\omega_{q-k})\,.$$

(3.35)

B. Crossed-box diagrams

The contribution of diagram 7 in Fig. 2 [for convenience redrawn in Fig. 4(a)] is given by

$$\langle\vec{q}'\Lambda_1'\Lambda_2'|M_1^c(z)|\vec{q}\Lambda_1\Lambda_2\rangle$$

$$=\frac{(4\pi)^2}{(2\pi)^6}g_\pi^2\frac{f_{N\Delta\pi}^2}{m_\pi^2}(2-\tfrac{2}{3}\vec{\tau}_1\cdot\vec{\tau}_2)$$

$$\times\sum_{h_1^*,h_2}\int\frac{d^3k\,\bar{u}_{\Lambda_2'}(-\vec{q}')i\gamma^5u_{h_2}(\vec{k}-\vec{q}-\vec{q}')\bar{u}_{h_2}(\vec{k}-\vec{q}-\vec{q}')i\gamma^5u_{\Lambda_2}(-\vec{q})F_{NN\pi}[(\vec{q}'-\vec{k})^2]F_{NN\pi}[(\vec{q}-\vec{k})^2]}{4\omega_{q-k}\omega_{q'-k}}$$

$$\times\frac{\bar{u}_{\Lambda_1'}(\vec{q}')i(q'-k)_\mu u_{h_1^*}^\mu(\vec{k})\bar{u}_{h_1^*}^\nu(\vec{k})i(k-q)_\nu u_{\Lambda_1}(\vec{q})F_{N\Delta\pi}[(\vec{q}'-\vec{k})^2]F_{N\Delta\pi}[(\vec{q}-\vec{k})^2]}{(z-E_{q'}-E_k^*-\omega_{q'-k})(z-E_{k-q-q'}-E_k^*-\omega_{q'-k}-\omega_{q-k})(z-E_q-E_k^*-\omega_{q-k})}\,.$$

(3.36)

The form factors $F_{NN\pi}$ and $F_{N\Delta\pi}$ are parametrized in the same way as before [see Eq. (3.5)].

The spin sum involving an intermediate nucleon is now given by

$$\sum_{h_2}\bar{u}_{\Lambda_2'}(-\vec{q}')i\gamma^5u_{h_2}(\vec{k}-\vec{q}-\vec{q}')\bar{u}_{h_2}(\vec{k}-\vec{q}-\vec{q}')i\gamma^5u_{\Lambda_2}(-\vec{q})$$

$$=-\bar{u}_{\Lambda_2'}(-\vec{q}')\gamma^5\Lambda_+(\vec{k}-\vec{q}-\vec{q}')\gamma^5u_{\Lambda_2}(-\vec{q})$$

$$=\frac{1}{2E_{k-q-q'}}\bar{u}_{\Lambda_2'}(-\vec{q}')[\gamma^0E_{k-q-q'}+\vec{\gamma}\cdot(\vec{k}-\vec{q}-\vec{q}')-m]u_{\Lambda_2}(-\vec{q})$$

$$=\frac{1}{2E_{k-q-q'}}\bar{u}_{\Lambda_2'}(-\vec{q}')[\gamma^0(E_{k-q-q'}-(1-a)E_q-(1-b)E_{q'})+(1-a-b)m+c\gamma^2]u_{\Lambda_2}(-\vec{q})\,,$$

(3.37)

where use has been made of Eq. (3.14) and the Dirac equation. Comparison with Eq. (3.15) shows that Eq. (3.37) differs from the corresponding spin sum occurring in the stretched-box diagrams essentially by an overall sign and in the γ^0 factor. Since the spin sum involving the Δ isobar is the same as before, we obtain

$$\langle\vec{q}'\Lambda_1'\Lambda_2'|M_1^c(z)|\vec{q}\Lambda_1\Lambda_2\rangle=\frac{(4\pi)^2}{(2\pi)^6}g_\pi^2\frac{f_{N\Delta\pi}^2}{m_\pi^2}(2-\tfrac{2}{3}\vec{\tau}_1\cdot\vec{\tau}_2)$$

$$\times\int\frac{d^3k(Z_1'+Z_2'+Z_3'+Z_4')F_{NN\pi}[(\vec{q}'-\vec{k})^2]F_{NN\pi}[(\vec{q}-\vec{k})^2]F_{N\Delta\pi}[(\vec{q}'-\vec{k})^2]F_{N\Delta\pi}[(\vec{q}-\vec{k})^2]}{4\omega_{q'-k}\omega_{q-k}D_1^c}\,,$$

(3.38)

where

$$D_1^c=(z-E_{q'}-E_k^*-\omega_{q'-k})(z-E_{k-q-q'}-E_k^*-\omega_{q'-k}-\omega_{q-k})(z-E_q-E_k^*-\omega_{q-k})$$

(3.39)

and the Z_i' can be obtained from the Z_i [Eqs. (3.18), (3.22), (3.25), and (3.26)] by (i) changing the overall sign, (ii) replacing E_k by $E_{k-q-q'}$, (iii) replacing d_2 [Eq. (3.19)] by

$$d_2=E_{k-q-q'}-(1-a)E_q-(1-b)E_{q'}\,.$$

(3.40)

Again, the expressions have been symmetrized by using the fact that Fig. 4(b) should give a result identi-

cal to Fig. 4(a).

The other five crossed-box diagrams of Fig. 2 give the same result apart from the energy denominators. In the order of Fig. 2, D_1^c in Eq. (3.38) has to be replaced by

$$D_2^c = (z - E_{k-q-q'} - E_{q'} - \omega_{q-k})(z - E_k^* - E_{k-q-q'} - \omega_{q-k} - \omega_{q'-k})(z - E_{k-q-q'} - E_q - \omega_{q'-k}),$$

$$D_3^c = (z - E_{k-q-q'} - E_{q'} - \omega_{q-k})(z - E_k^* - E_{k-q-q'} - \omega_{q-k} - \omega_{q'-k})(z - E_k^* - E_q - \omega_{q-k}),$$

$$D_4^c = (z - E_k^* - E_{q'} - \omega_{q'-k})(z - E_k^* - E_{k-q-q'} - \omega_{q-k} - \omega_{q'-k})(z - E_q - E_{k-q-q'} - \omega_{q'-k}),$$ $\qquad$ (3.41)

$$D_5^c = (z - E_{q'} - E_{k-q-q'} - \omega_{q-k})(z - E_{q'} - E_q - \omega_{q-k} - \omega_{q'-k})(z - E_k^* - E_q - \omega_{q-k}),$$

$$D_6^c = (z - E_{q'} - E_k^* - \omega_{q'-k})(z - E_{q'} - E_q - \omega_{q-k} - \omega_{q'-k})(z - E_{k-q-q'} - E_q - \omega_{q'-k}).$$

Thus the total sum of the crossed-box diagrams of Fig. 2 plus those in which the isobar appears on the right hand side (giving an additional factor of 2) can be written as

$$\langle \vec{q}' \Lambda_1' \Lambda_2' | M^c(z) | \vec{q} \Lambda_1 \Lambda_2 \rangle = 2 \frac{(4\pi)^2}{(2\pi)^6} g_r^2 \frac{f_{N\Delta\pi}^2}{m_\pi^2} (2 - \tfrac{2}{3}\vec{\tau}_1 \cdot \vec{\tau}_2)$$

$$\times \int \frac{d^3k (Z_1' + Z_2' + Z_3' + Z_4') F_{NN\pi}[(\vec{q}' - \vec{k})^2] F_{NN\pi}[(\vec{q} - \vec{k})^2] F_{N\Delta\pi}[(\vec{q}' - \vec{k})^2] \cdot F_{N\Delta\pi}[(\vec{q} - \vec{k})^2]}{4\omega_{q'-k}\omega_{q-k} D^c},$$

$\qquad$ (3.42)

where

$$\frac{1}{D^c} = \sum_{i=1}^{6} \frac{1}{D_i^c}.$$ $\qquad$ (3.43)

For the actual numerical calculations, we need the partial wave amplitudes

$$\langle \Lambda_1' \Lambda_2' | M^{b,J}(q',q|z) | \Lambda_1 \Lambda_2 \rangle = 2\pi \int_{-1}^{+1} d(\cos\theta) d_{\Lambda\Lambda'}^J(\theta) \langle \vec{q}' \Lambda_1' \Lambda_2' | M^b(z) | \vec{q} \Lambda_1 \Lambda_2 \rangle$$ $\qquad$ (3.44)

and

$$\langle \Lambda_1' \Lambda_2' | M^{c,J}(q',q|z) | \Lambda_1 \Lambda_2 \rangle = 2\pi \int_{-1}^{+1} d(\cos\theta) d_{\Lambda\Lambda'}^J(\theta) \langle q' \Lambda_1' \Lambda_2' | M^c(z) | q \Lambda_1 \Lambda_2 \rangle,$$ $\qquad$ (3.45)

where $d_{\Lambda\Lambda'}^J(\theta)$ are the usual reduced rotation matrices, $\Lambda = \Lambda_1 - \Lambda_2$ and $\Lambda' = \Lambda_1' - \Lambda_2'$. The expressions (3.44) and (3.45) are evaluated numerically.

IV. RESULTS AND DISCUSSIONS

A. Noniterative isobar diagrams

In this section, we will first present numerical results of stretched-box and crossed-box $N\Delta$ diagrams, evaluated analytically in the last chapter,
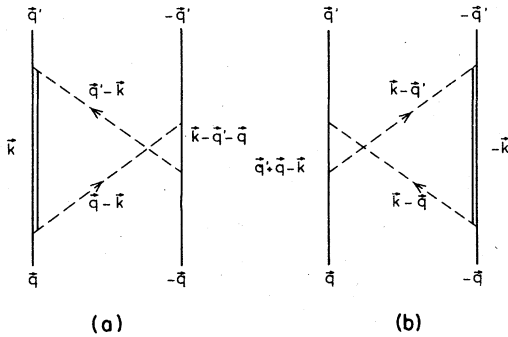

(o) $\qquad\qquad$ (b)

FIG. 4. Selected crossed-box diagrams displaying the notation as it is used in the text.

and compare them with the results of the corresponding iterative diagrams, described already in Ref. 15. The evaluation of the noniterative diagrams is much more involved since meson energies occur in all propagators. This makes the use of suitable transition potentials as in Ref. 15 impossible. Therefore it is not surprising that people have looked for reasonable approximations, in which the exact evaluation of noniterative diagrams can be avoided. The existence of such approximations is suggested by the special isospin structure of box and crossed-box diagrams.[14] Namely, the sum of all time orderings of Fig. 2 is given by

$$A_{N\Delta} = (2 + \tfrac{2}{3}\vec{\tau}_1 \cdot \vec{\tau}_2) B_{N\Delta} + (2 - \tfrac{2}{3}\vec{\tau}_1 \cdot \vec{\tau}_2) C_{N\Delta}. \qquad (4.1)$$

Here, $(2 + \tfrac{2}{3}\vec{\tau}_1 \cdot \vec{\tau}_2) B_{N\Delta}$ denotes the contribution of all box diagrams (1–6 of Fig. 3), whereas $(2 - \tfrac{2}{3}\vec{\tau}_1 \cdot \vec{\tau}_2) C_{N\Delta}$ stands for the contribution of all crossed-box diagrams (7–12 of Fig. 2). Equation (4.1) can be rewritten as
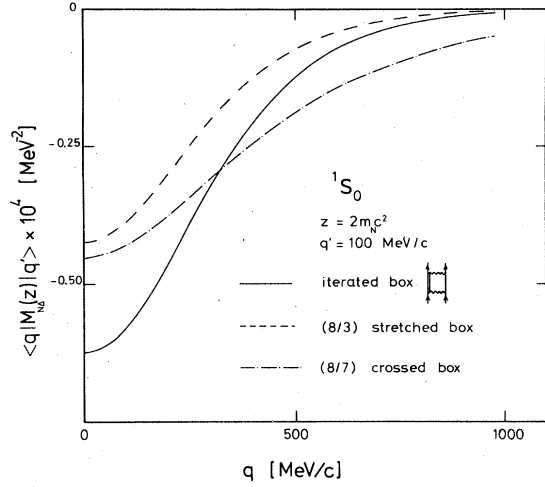
FIG. 5. Matrix elements $\langle q \,|\, M_{N\Delta}^{\pi'}(z) \,|\, q'\rangle$ in the $^1S_0$ channel are displayed as a function of q. The value of q' has been fixed to $q' = 100$ MeV/c and the starting energy $z = 2m$. For this figure the isospin factors have been dropped. The parameters of $M_{N\Delta}^{\pi'}$ are given in Table I using, however, a cutoff mass $\Lambda_{\pi}' = 800$ MeV. The dashed line displays the contributions of stretched-box diagrams multiplied by a factor of $\frac{8}{3}$. The dashed-dotted curve shows the contributions of crossed-box diagrams multiplied by a factor of $\frac{8}{7}$. For comparison the solid line gives the contribution of the corresponding iterative diagrams.
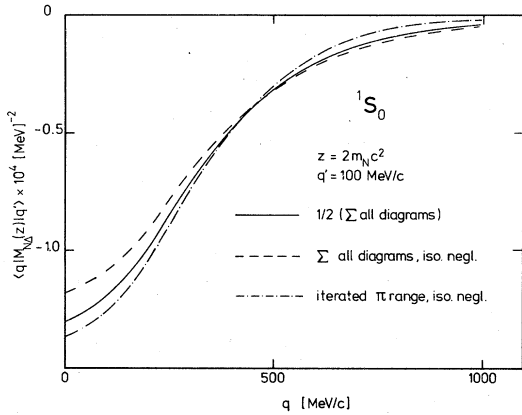
FIG. 6. Matrix elements $\langle q \,|\, M_{N\Delta}^{\pi'}(z) \,|\, q'\rangle$ in the $^1S_0$ channel. The dashed curve represents the result for the sum of all crossed and uncrossed diagrams with intermediate $N\Delta$ states. The dashed-dotted curve displays the result for the iterated pion-range transition potential. While for these two curves the isospin factors are neglected, they are taken into account in calculating the sum of all diagrams, as shown in the solid curve. The solid curve has been renormalized by multiplying with $\frac{1}{2}$, in order to allow a comparison with the dashed-dotted curve. For further details, see Fig. 5.
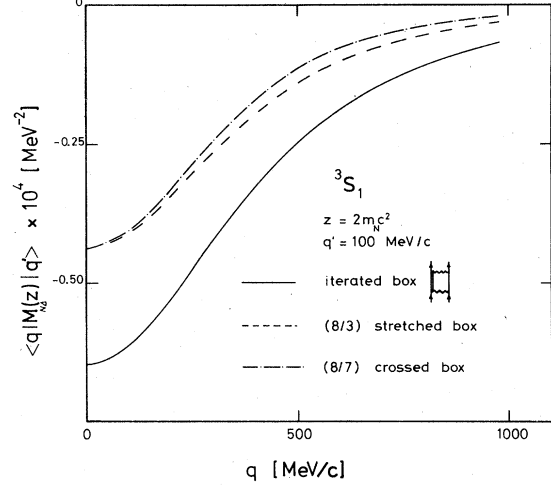

FIG. 7. Matrix elements $\langle q \,|\, M_{N\Delta}^{\pi'}(z) \,|\, q'\rangle$ in the $^3S_1$ channel. For further details, see Fig. 5.

$$A_{N\Delta} = 2(B_{N\Delta} + C_{N\Delta}) + \tfrac{2}{3}\vec{\tau}_1 \cdot \vec{\tau}_2 (B_{N\Delta} - C_{N\Delta}). \qquad (4.2)$$

If $C_{N\Delta}$ is comparable to $B_{N\Delta}$, the following approximation is suggested, which consists of two steps:

(i) Replace $(B_{N\Delta} + C_{N\Delta})$ by the second iteration of pion-range transition potentials, denoted by $B_{N\Delta}'$. (The use of $B_{N\Delta}'$ overestimates $B_{N\Delta}$ alone by roughly a factor of 2, as mentioned already in the Introduction).

(ii) Neglect the $(B_{N\Delta} - C_{N\Delta})$ term compared to the first term. This leads to
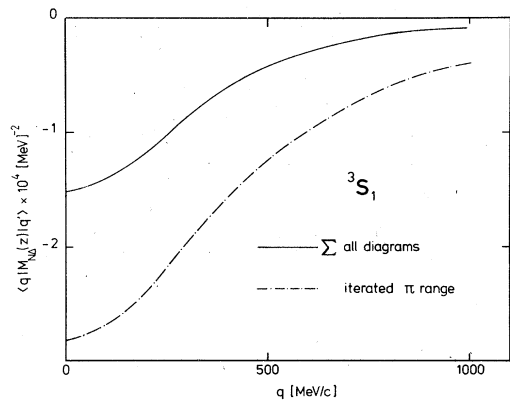
$$A_{N\Delta} \simeq 2B_{N\Delta}', \qquad (4.3)$$

FIG. 8. Matrix elements $\langle q \,|\, M_{N\Delta}^{\pi'}(z) \,|\, q'\rangle$ in the $^3S_1$ channel. The solid curve shows the total result for all $N\Delta$ diagrams including isospin factors. Since the isospin factors for uncrossed diagrams vanish for this channel, this result originates from crossed-box terms only. The dashed-dotted curve displays the result for the isoscalar part (factor of 2) of the iterated pion-range potential. For further details, see Fig. 5.

i.e., the exact contribution is replaced by the iso-scalar part of (twice-iterated) pion-range transition potentials. The main aim of this section is to test this approximation. We first investigate the basic assumption that $B_{N\Delta}$ is comparable to $C_{N\Delta}$. Consequently, isospin factors are dropped in the following discussion. It has been pointed out in Ref. 14 that, if all particles are considered to be at rest (i.e., energies are replaced by corresponding masses), the stretched-box (crossed-box) diagrams of Fig. 2 are $\frac{3}{8}$ ($\frac{7}{8}$) of the iterative ones. This implies that $C_{N\Delta}$ is only about $\frac{2}{3}$ of $B_{N\Delta}$. It is not surprising, however, that the correct result (for which the restriction to particles at rest has to be given up) is typically different, as demonstrated in Fig. 5 for the $^1S_0$ channel. First, the stretched-box diagrams are smaller. Obviously, recoil effects suppress the noniterative contributions more strongly than the iterative ones. Furthermore, the simple estimate underestimates the exact crossed-box result for higher values of q. (This shows that the crossed-box terms are of shorter range than the iterative terms and should be more suppressed in higher partial waves). In fact, for $q = 500$ MeV, $C_{N\Delta}$ roughly agrees with $B_{N\Delta}$. Thus, in contrast to the simple estimate, our exact calculations justify the above assumption in the $^1S_0$ state.

We now investigate the replacement of ($B_{N\Delta}$ $+ C_{N\Delta}$) by $B'_{N\Delta}$ in the same channel. Figure 6 demonstrates that the overall strength of ($B_{N\Delta} + C_{N\Delta}$) (dashed curve) can be fairly well reproduced by iterated pion-range potentials (dash-dot curve), which, however, yields a contribution of longer range, as expected. From the above discussion it is then not surprising that $\frac{1}{2}A_{N\Delta}$ (solid line) is well approximated by $B'_{N\Delta}$ (dash-dot line) [see Eq. (4.3)].

Unfortunately, the situation is not so nice in the other partial waves. In $^3S_1$, ($B_{N\Delta} + C_{N\Delta}$) is again fairly well approximated by $B'_{N\Delta}$ (compare Fig. 7 with Fig. 8). However, $C_{N\Delta}$ is now only $\frac{1}{2}$ of $B_{N\Delta}$. Moreover, $\vec{\tau}_1 \cdot \vec{\tau}_2$ now has the eigenvalue -3 (compared to 1 in $^1S_0$). Consequently, the ($B_{N\Delta} - C_{N\Delta}$) term in Eq. (4.2) cannot be neglected in this partial wave. This is confirmed in Fig. 8, which compares $A_{N\Delta}$ with $2B'_{N\Delta}$. Obviously, the isoscalar part of the twice-iterated pion-range transition potentials grossly overestimates the exact result.

Our calculations have shown that the same is true for nearly all higher partial waves ($L \geqslant 1$). The main reason is that the realistic contributions, being of shorter range due to the inclusion of recoil terms, are much more suppressed in these partial waves than contributions with pion range.

In a simple coupled-channel treatment (see Ref.

13) ($B_{N\Delta} - C_{N\Delta}$) is also replaced by $B'_{N\Delta}$, leading to

$$A_{N\Delta} \simeq (2 + \tfrac{2}{3}\vec{\tau}_1 \cdot \vec{\tau}_2)B'_{N\Delta}, \tag{4.4}$$

i.e., a transition potential of pion range is used also for the isovector piece. From the above discussion it should be clear that Eq. (4.4) is a bad approximation, leading, in fact, to a vanishing contribution in isospin-zero states. Consequently, in $^3S_1$, the true results lies between the prescriptions of (a) including and (b) neglecting the isovector part in the iterated transition potentials of pion range.

However, according to the work of Smith and Pandharipande,[22] the isovector part might ultimately become quite small if not only $N\Delta$ but also NN and $\Delta\Delta$ contributions are considered. The argument goes as follows: The total contribution $A = A_{NN} + A_{N\Delta} + A_{\Delta\Delta}$ is given by

$$\begin{aligned} A = &(3 - 2\vec{\tau}_1 \cdot \vec{\tau}_2)B_{NN} + (3 + 2\vec{\tau}_1 \cdot \vec{\tau}_2)C_{NN} \\ &+ (2 + \tfrac{2}{3}\vec{\tau}_1 \cdot \vec{\tau}_2)B_{N\Delta} + (2 - \tfrac{2}{3}\vec{\tau}_1 \cdot \vec{\tau}_2)C_{N\Delta} \\ &+ (\tfrac{4}{3} - \tfrac{2}{9}\vec{\tau}_1 \cdot \vec{\tau}_2)B_{\Delta\Delta} + (\tfrac{4}{3} + \tfrac{2}{9}\vec{\tau}_1 \cdot \vec{\tau}_2)C_{\Delta\Delta}. \end{aligned} \tag{4.5}$$

A regrouping of terms yields

$$\begin{aligned} A = &(- 2\vec{\tau}_1 \cdot \vec{\tau}_2)(B_{NN} + C_{NN}) + 4\vec{\tau}_1 \cdot \vec{\tau}_2 C_{NN} \\ &+ (2 + \tfrac{2}{3}\vec{\tau}_1 \cdot \vec{\tau}_2)(B_{N\Delta} + C_{N\Delta}) - \tfrac{4}{3}\vec{\tau}_1 \cdot \vec{\tau}_2 C_{N\Delta} \\ &+ (\tfrac{4}{3} - \tfrac{2}{9}\vec{\tau}_1 \cdot \vec{\tau}_2)(B_{\Delta\Delta} + C_{\Delta\Delta}) + \tfrac{4}{9}\vec{\tau}_1 \cdot \vec{\tau}_2 C_{\Delta\Delta}. \end{aligned} \tag{4.6}$$

The authors of Ref. 22 have demonstrated that the replacement of $B + C$ by B', i.e., by (twice-iterated) pion-range potentials is, in fact, a reasonable approximation not only for $N\Delta$, but also for NN and $\Delta\Delta$. Therefore

$$\begin{aligned} A \simeq &(3 - 2\vec{\tau}_1 \cdot \vec{\tau}_2)B'_{NN} + (2 + \tfrac{2}{3}\vec{\tau}_1 \cdot \vec{\tau}_2)B'_{N\Delta} \\ &+ (\tfrac{4}{3} - \tfrac{2}{9}\vec{\tau}_1 \cdot \vec{\tau}_2)B'_{\Delta\Delta} + 4(C_{NN} - \tfrac{1}{3}C_{N\Delta} + \tfrac{1}{9}C_{\Delta\Delta})\vec{\tau}_1 \cdot \vec{\tau}_2. \end{aligned} \tag{4.7}$$

Now, again following Ref. 22, the C terms (being separately appreciable) cancel to a remarkable degree leading to

$$\begin{aligned} A \simeq &(3 - 2\vec{\tau}_1 \cdot \vec{\tau}_2)B'_{NN} + (2 + \tfrac{2}{3}\vec{\tau}_1 \cdot \vec{\tau}_2)B'_{N\Delta} \\ &+ (\tfrac{4}{3} - \tfrac{2}{9}\vec{\tau}_1 \cdot \vec{\tau}_2)B'_{\Delta\Delta}. \end{aligned} \tag{4.8}$$

(This corresponds precisely to the procedure of the usual coupled-channel treatment; see Ref. 13.) If we finally make the (reasonable) assumption that there is a similar cancellation for the B terms, we arrive at

$$A \approx 3B'_{NN} + 2B'_{N\Delta} + \tfrac{4}{3}B'_{\Delta\Delta}, \tag{4.9}$$

which implies that the total isovector term is quite small.

Summarizing, we have shown that the $N\Delta$ contribution cannot be described in a realistic way

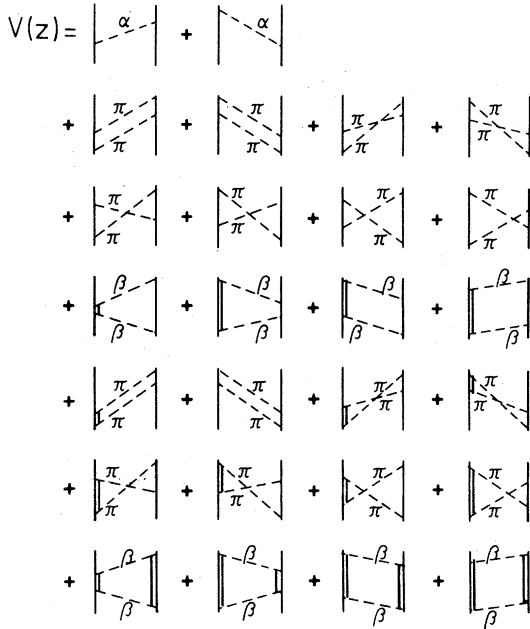$$V(z) = \left[\cdots \alpha \cdots \right] + \left[\cdots \alpha \cdots \right]$$

FIG. 9. Diagrams included in the model of Eq. (4.10). The solid lines denote nucleons, the double-solid line denotes a Δ isobar. The α stands for π, η, σ, δ, ρ, and ω mesons, while β only for π and ρ mesons. Corresponding diagrams where the Δ appears on the right-hand side are not shown explicitly but are included in the calculations.
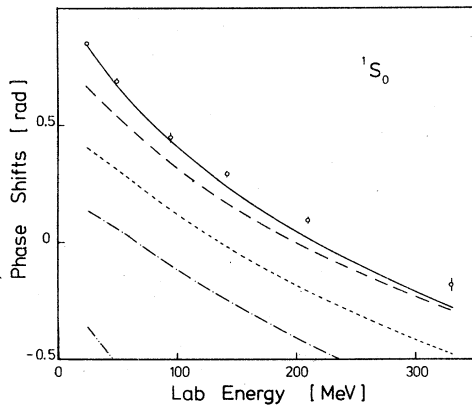
FIG. 10. $^1S_0$ nucleon-nucleon phase shifts (in rad) as a function of the nucleon lab energy (in MeV). The experimental values are taken from the energy-independent Livermore analysis (Ref. 24). Results for the full V_{eff} of Eq. (4.10) are denoted by the solid curve. For the dashed curve, M'^{π}_{NN} has been omitted, while in calculating the dotted curve $M'^{\pi}_{NN} + M'^{\pi}_{N\Delta}$ has been omitted. The dashed-dotted curve contains the OBE part of Eq. (4.10) (V_{OBE}) only, whereas the dashed-double-dotted curve is obtained when, in addition, even the contribution from σ exchange is omitted.
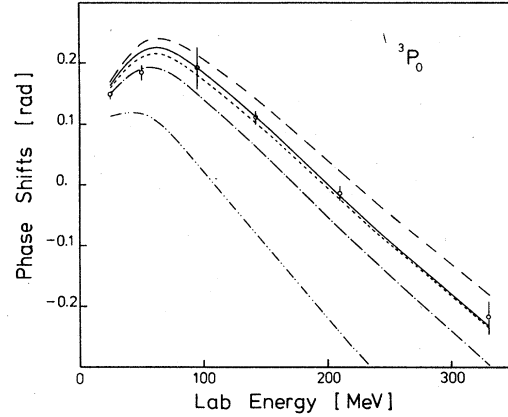
FIG. 11. $^3P_0$ phase shifts. For further details, see Fig. 10.

for all partial waves by using pion-range transition potentials and dropping the isovector part. First, the longer range of such transition potentials leads to an overestimate of the true result in $(L \geqslant 1)$ partial waves. Second, it is only through the consideration of NN, $N\Delta$, and $\Delta\Delta$ contributions at the same time that the total isovector term is possibly small.

B. Effects in *NN* scattering

In order to show the effect of these noniterative diagrams on nucleon-nucleon scattering phase shifts, we use as effective potential

$$V_{\text{eff}}(z) = V_{\text{OBE}}(z) + M_{N\Delta}(z) + M_{\Delta\Delta}(z)$$
$$+ M'^{\pi}_{NN}(z) + M'^{\pi}_{N\Delta}(z) . \tag{4.10}$$

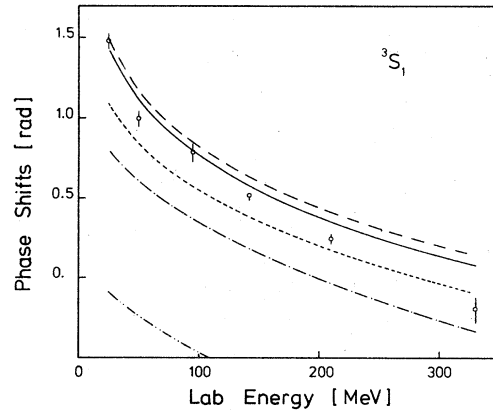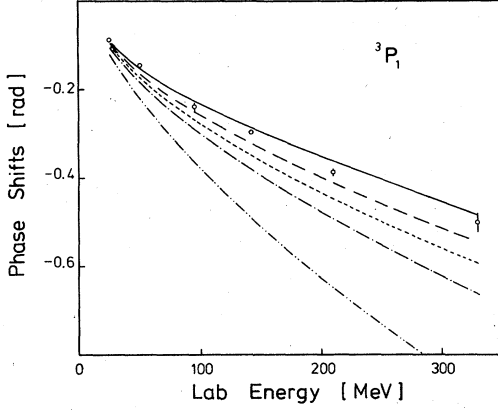FIG. 12. $^3S_1$ phase shifts. For further details, see FIG. 10.

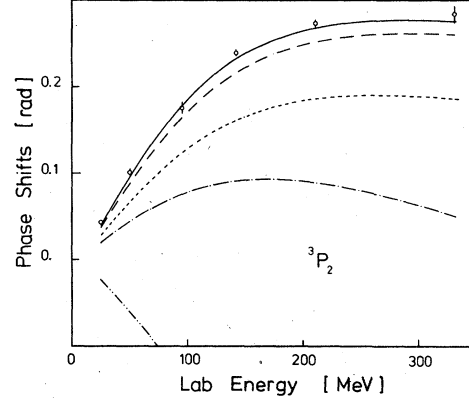FIG. 13. $^3P_1$ phase shifts. For further details, see Fig. 10.

FIG. 14. $^3P_2$ phase shifts. For further details, see Fig. 10.

Here, V_{OBE} is the one-boson-exchange potential of Kotthoff et al.[23] (using now $F_\alpha \equiv (\Lambda_\alpha{}^2 - m_\alpha{}^2)/[\Lambda_\alpha{}^2 + (q' - q)^2]$ at all vertices). $M_{N\Delta}, M_{\Delta\Delta}$ denotes the sum of iterative diagrams with $N\Delta(\Delta\Delta)$ intermediate states including π and ρ exchange.[15] $M_{NN}^{\prime\pi}$ denotes the sum of noniterative diagrams with NN intermediate states including only π-exchange,[17] whereas $M_{N\Delta}^{\prime\pi}$ denotes the sum of noniterative diagrams with $N\Delta$ intermediate states discussed explicitly in the foregoing chapter. The correspond-

ing diagrams of $V_{eff}(z)$ [Eq. (4.10)] are shown in Fig. 9.

The R matrix is then obtained from

$$R(z) = V_{eff}(z) + V_{eff}(z) \frac{\mathrm{P}}{z - H_0} R(z),   (4.11)$$

where P denotes the principal value. Explicitly, we obtain, in partial waves and helicity-state basis,

$$\langle \Lambda_1' \Lambda_2' | R^J(q',q|z) | \Lambda_1 \Lambda_2 \rangle = \langle \Lambda_1' \Lambda_2' | V_{eff}^J(q',q|z) | \Lambda_1 \Lambda_2 \rangle$$

$$+ \sum_{h_1, h_2} \mathrm{P} \int_0^\infty \frac{dk\, k^2}{z - 2E_k} \langle \Lambda_1' \Lambda_2' | V_{eff}^J(q',k|z) | h_1 h_2 \rangle \langle h_1 h_2 | R^J(k,q|z) | \Lambda_1 \Lambda_2 \rangle.   (4.12)$$

Here $z = 2E_q$. The NN scattering phase shifts can be obtained from R^J in the usual way; see, e.g., Ref. 11.

The meson parameters are shown in Table I. They are partly adjusted in order to obtain a reasonable description of the NN scattering phase shifts. In the explicit higher-order diagrams,

we use throughout $\Lambda_\pi = 1$ GeV, whereas the fit requires $\Lambda_\pi = 1.4$ GeV in V_{OBE}. We feel justified to use different values for Λ_π at the present stage. In our model, the form factors still have to be considered to be essentially phenomenological quantities, which effectively replace contributions still not included in the present model. For

TABLE I. Parameters for $V_{eff}(z)$ [Eq. (4.1)]. m_α and Λ_α are given in MeV. The number in parentheses denotes the ratio of coupling constants $f_{NN\rho}/g_{NN\rho}$. Λ_α denotes the cutoff mass in the OBE vertices, whereas Λ_α' denotes the cutoff mass at all other vertices. All form factors are parametrized according to Eq. (3.5).

	π	η	σ	δ	ω	ρ
$g_{NN\alpha}{}^2$	14.4	8.4	15.902	0.451	30	0.78 (4.85)
m_α	138	548.5	650	960	782.8	763
Λ_α	1400	1400	1400	1400	1400	1400
Λ_α'	1000					1500
$f_{N\Delta\alpha}{}^2$	0.23					15.08

TABLE II. Low energy scattering and deuteron data.

	Expt.	Present model [Eq. (4.1)]
E (MeV)	2.22462 ± 0.00006	2.2238
Q (fm^2)	0.2860 ± 0.0015	0.2871
P_D (%)	5 ± 2	3.78
a_s (fm)	-23.715 ± 0.015	-23.86
r_s (fm)	2.73 ± 0.03	2.68
a_t (fm)	5.423 ± 0.005	5.39
r_t (fm)	1.748 ± 0.014	1.74

example, the inclusion of explicit 3π-exchange diagrams, which are expected to influence the inner part of the tensor force, might ultimately make it possible to use $\Lambda_\pi = 1$ GeV (which is suggested by independent information) throughout. Note that, due to their short range, a reliable theoretical description of form factors might require taking into account quark-theoretical viewpoints, which is only in its infancy at present.

The resulting low-energy parameters are shown in Table II, while some important partial wave phase shifts are presented in Figs. 10–16. The solid lines are obtained when $V_{\rm eff}$ [Eq. (4.10)] is used in Eq. (4.12). The dashed lines result when $M_{NN}'^\pi$ is omitted; for the dotted line $(M_{NN}'^\pi + M_{NN}'^\pi)$ is omitted; the dashed-dotted curve is obtained through the use of $V_{\rm OBE}$ only; and finally the dashed-double-dotted curve is obtained when omitting, in addition, the σ contribution in $V_{\rm OBE}$. This part is supposed to take into account the rest of the 2π exchange which is not yet described explicitly in our model. The experimental values are taken from the Livermore analysis.[24]

Obviously, a good agreement with empirical

TABLE III. Nuclear bare phase shifts (in rad) obtained with $V_{\rm eff}(z)$ [Eq. (4.10)].

$E_{\rm lab}$ (MeV)	25	50	95	142	210	330
$^1S_0$	0.837	0.667	0.430	0.238	0.017	-0.279
$^3P_0$	0.164	0.219	0.192	0.112	-0.019	-0.233
$^1P_1$	-0.110	-0.154	-0.185	-0.199	-0.210	-0.221
$^3P_1$	-0.094	-0.154	-0.227	-0.287	-0.362	-0.485
$^3S_1$	1.420	1.112	0.795	0.576	0.348	0.075
ϵ_1	0.023	0.019	0.009	-0.001	-0.013	-0.030
$^3D_1$	-0.051	-0.119	-0.220	-0.299	-0.380	-0.470
$^1D_2$	0.013	0.029	0.059	0.089	0.127	0.163
$^3D_2$	0.067	0.160	0.290	0.374	0.431	0.429
$^3P_2$	0.040	0.096	0.179	0.232	0.268	0.276
ϵ_2	-0.015	-0.031	-0.047	-0.050	-0.043	-0.021
$^3F_2$	0.002	0.005	0.009	0.010	0.003	-0.028
$^1F_3$	-0.008	-0.021	-0.040	-0.053	-0.066	-0.089
$^3F_3$	-0.004	-0.013	-0.028	-0.042	-0.059	-0.084
$^3D_3$	-0.001	-0.002	0.002	0.010	0.023	0.034
ϵ_3	0.010	0.030	0.062	0.087	0.112	0.136
$^3G_3$	-0.001	-0.005	-0.017	-0.033	-0.058	-0.101
$^1G_4$	0.001	0.003	0.007	0.010	0.015	0.024
$^3G_4$	0.003	0.013	0.037	0.061	0.092	0.134
$^3F_4$	0.000	0.002	0.005	0.011	0.021	0.039
$^3H_4$	0.000	0.000	0.002	0.003	0.005	0.006
ϵ_4	-0.001	-0.003	-0.004	-0.015	-0.021	-0.029

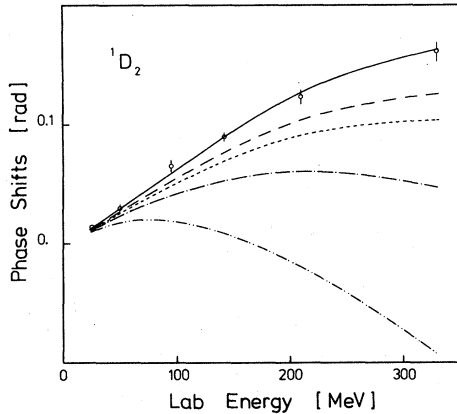FIG. 15. $^1D_2$ phase shifts. For further details, see Fig. 10.

FIG. 16. $^3D_2$ phase shifts. For further details, see Fig. 10.

phase shifts is obtained. Compared to OBE models, the $^3D_2$ phase shifts are lowered considerably, i.e., there is a strong improvement. The main reason can be traced back to the behavior of $M_{\Delta\Delta}$: it is sizably attractive in $^3S_1$; however, because of its short range, it is negligible in $^3D_2$. Consequently, the attraction in $^3D_2$ is now reduced compared to $^3S_1$, i.e., the $^3D_2$ phase shifts are lowered. Our model replaces part of the exactly isoscalar σ exchange by explicit diagrams which are only roughly isoscalar. Namely, the isospin-zero contribution is slightly shorter ranged (because of the dominance of crossed-box diagrams in this channel) and is thus more suppressed in higher partial waves.

Concerning the noniterative isobar diagrams $(M_{N\Delta}'^{\pi})$, the figures clearly demonstrate that they are as important as isobar box diagrams $(M_{N\Delta} + M_{\Delta\Delta})$. (We believe that ρ exchange will not drastically reduce the importance of $M_{N\Delta}'^{\pi}$). Especially in isospin-zero states (where $M_{N\Delta}$ does not contribute), the isobar contribution is drastically enlarged; see, e.g., $^3D_2$. Consequently, the inclusion of $M_{N\Delta}'^{\pi}$ in the evaluation of the Δ probability of the deuteron, which has not been done so far, should lead to a considerable enhancement, too. For convenience, we present in Table III the numerical values of the nuclear bare phase shifts obtained with V_{eff} [Eq. (4.10)] for $J \leqslant 4$.
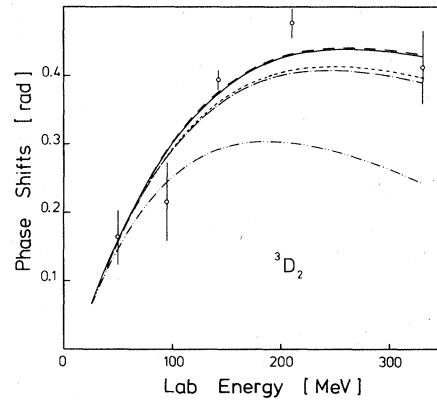
V. SUMMARY

We have explicitly evaluated the formalism for the calculation of the noniterative diagrams involving $N\Delta$ intermediate states. It is shown that such diagrams can only crudely be taken into account by using a transition potential of pion range and dropping the isovector part. For example, it grossly overestimates the isobar contribution in the $^3S_1$ channel. Furthermore, we demonstrate explicitly that the noniterative diagrams are as important as isobar box diagrams.

In our model, the explicit 2π-exchange diagrams $(M_{N\Delta} + M_{\Delta\Delta} + M_{NN}'^{\pi} + M_{N\Delta}'^{\pi})$ replace roughly 50% of the σ exchange providing the intermediate-range attraction in OBE models. The other part is mainly given by rescattering contributions (involving diagrams in which the two exchanged pions interact). They must be included before a realistic and explicit model for the total 2π-exchange contribution is obtained, which in two-body scattering agrees satisfactorily with the result of dispersion-theoretic models. In the present model, the rescattering part is still effectively described by σ exchange. We expect, however, that the main modification of the 2π-exchange contribution in the nuclear medium occurs in those diagrams already described explicitly.

[1]R. V. Reid, Ann. Phys. (N. Y.) **50**, 411 (1968).

[2]B. D. Day, Rev. Mod. Phys. **39**, 719 (1967).

[3]H. A. Bethe, Annu. Rev. Nucl. Sci. **21**, 93 (1971).

[4]B. D. Day, Rev. Mod. Phys. **50**, 495 (1978); Nucl. Phys. **A328**, 1 (1979).

[5]V. R. Pandharipande and R. B. Wiringa, Rev. Mod. Phys. **51**, 821 (1979).

[6]A. C. Phillips, Rep. Prog. Phys. **40**, 905 (1977).

[7]J. G. Zabolitzky, Nucl. Phys. **A228**, 285 (1974).

[8]A. Faessler, H. Müther, K. Shimizu, and W. Wadia,

Nucl. Phys. A333, 428 (1980).

[9]K. Holinde, Nucl. Phys. A328, 439 (1979).

[10]H. Arenhövel and W. Fabian, Nucl. Phys. A282, 397 (1977); E. L. Lomon, Phys. Lett. 68B, 419 (1977).

[11]K. Erkelenz, Phys. Rep. 13C, 191 (1974); K. Holinde and R. Machleidt, Nucl. Phys. A247, 495 (1975); A256, 479 (1976); A256, 497 (1976).

[12]M. Lacombe, B. Loiseau, J. M. Richard, R. Vinh Mau, P. Pires, and R. de Tourreil, Phys. Rev. D 12, 1495 (1975); A. D. Jackson, D. O. Riska, and B. Verwest, Nucl. Phys. A249, 397 (1975).

[13]A. M. Green, Rep. Prog. Phys. 39, 1109 (1976).

[14]J. W. Durso, M. Saarela, G. E. Brown, and A. D. Jackson, Nucl. Phys. A278, 445 (1977).

[15]K. Holinde, R. Machleidt, M. R. Anastasio, A. Faessler, and H. Müther, Phys. Rev. C 18, 870 (1978).

[16]M. R. Anastasio, A. Faessler, H. Müther, K. Holinde, and R. Machleidt, Phys. Rev. C 18, 2416 (1978).

[17]K. Holinde, R. Machleidt, M. R. Anastasio, A. Faessler, and H. Müther, Phys. Rev. C 19, 948 (1979).

[18]H. Müther, A. Faessler, M. R. Anastasio, K. Holinde, and R. Machleidt, Phys. Rev. C 22, 1744 (1980).

[19]D. Schütte, Nucl. Phys. A221, 450 (1974).

[20]G. E. Brown, *Nucleon-Nucleon Interactions—1977 (Vancouver)*, Proceedings of the Second International Conference on Nucleon-Nucleon Interaction, edited by H. Fearing, D. Measday, and A. Strathdee (AIP, New York, 1978), p. 169.

[21]J. J. deSwart and M. M. Nagels, Fortschr. Phys. 28, 214 (1978).

[22]R. A. Smith and V. R. Pandharipande, Nucl. Phys. A256, 327 (1976).

[23]K. Kotthoff, K. Holinde, R. Machleidt, and D. Schütte, Nucl. Phys. A242, 429 (1975).

[24]M. McGregor, R. Arndt, and R. Wright, Phys. Rev. 182, 1714 (1969).